Examining the temporal evolution of induced seismicity sequences generated by long-term, low pressure fluid injections

Tom J. Watkins, James P. Verdon, Germán Rodríguez-Pradilla

Supplementary Material

This supplementary material provides further information about each of the case studies presented in the main paper. Figures S1 – S27 show the temporal evolution of magnitudes, the frequency-magnitude distribution, and the NRBE model results for each case study. In the attached zip file we provide earthquake catalogs in plain text format for each case study.

A note on magnitudes

The primary objective of this study is to examine the evolution of magnitudes within selected induced seismicity sequences. Self-evidently, this requires that the catalogs studied have accurate magnitude estimates. In some cases, the magnitudes have been provided as moment magnitude (M_W) and in some they are local magnitudes (M_L), or indeed other types of magnitude such as duration magnitudes (M_D). Throughout our study, we refer to these different scales generically as M.

We note that estimation of magnitudes of induced seismicity in industrial settings can be challenging (e.g., Butcher et al., 2017; Kendall et al., 2019; Kettlety et al., 2021). These challenges arise from a combination of different factors. While M_L and M_W should be roughly equivalent, at lower magnitudes ($M < 3.0$), M_L is systematically observed to be lower than M_W by a factor of approximately $2/3^{rds}$, caused by the attenuation of high frequencies from small-magnitude events (Butcher et al., 2020). In addition, different instrumental arrays are sometimes deployed during a given sequence (e.g., Kettlety et al., 2021), which can introduce bias to magnitude estimates especially if geophones with a limited frequency response are deployed (Viegas et al., 2012).

Induced earthquakes often occur within sedimentary basins, and may be detected on dedicated local monitoring arrays, resulting in ray-paths that are entirely through softer sedimentary rocks. In contrast, natural earthquakes typically occur deeper within the crust and are recorded on distant stations, resulting in ray-paths that are primarily through crystalline crustal rocks. As such, the attenuation experienced by seismic waves from induced events recorded on local monitoring arrays can be very different to that experienced by waves from natural earthquakes, meaning that long-used local magnitude scales do not produce accurate results for induced seismicity (e.g., Butcher et al., 2017).

However, the re-calculation of magnitudes from waveform data is beyond the scope of this study. We have used the magnitudes provided in the catalogs described below without any independent quality control.

Castor, Gulf of Valencia, Spain

The seismicity at the Castor NGS facility has been described by Cesca et al. (2014; 2021); Ruiz-Barajas et al. (2017); and Vilarrasa et al. (2021). The target reservoir was the Amposta oilfield in the Gulf of Valencia, approximately 20 km offshore at a depth of 1.7 km. The oilfield was discovered in 1970, and produced from 1973 to 1989. After the field was abandoned, it was redeveloped as an NGS site. Injection of cushion gas for NGS commenced on the 02/09/2013. Three days after the beginning of injection, seismicity began to occur, with the largest events being felt by the public living along the coast, causing significant concerns. Gas injection was stopped on the 16/09/2013. Seismicity continued after the cessation of injection until late October 2013, with the largest events (M > 4.0) occurring as trailing events. The catalog we use in this study is drawn from the supplementary materials published by Cesca et al. (2021). Information about injection start and stop times is drawn from the aforementioned publications.

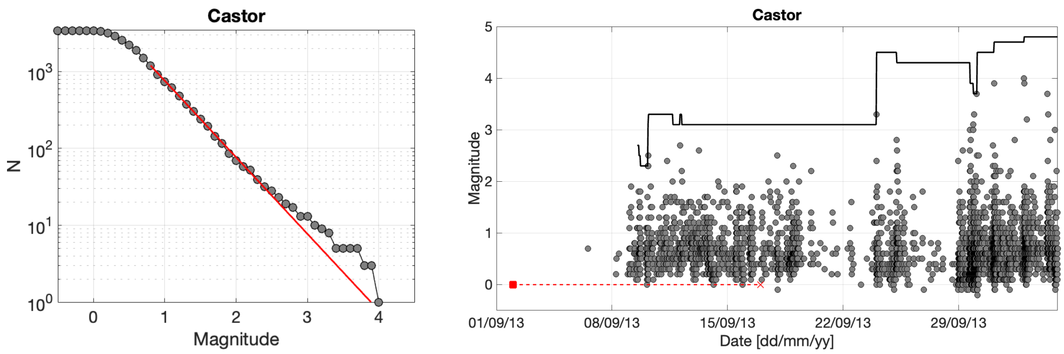

(a) *(b)*

Figure S1: Frequency-magnitude distribution for the Castor sequence (a) and the temporal evolution of magnitudes (b). In (a), the red line shows the GR fit. In (b), the red square shows the onset of injection, and the cross shows the end of injection. The black line shows the results of the NRBE forecast. This figure format is used in Figures S2 to S27.

Puerto Gaitán, Llanos Basin, Colombia

The Puerto Gaitán seismicity sequence is described by Molina et al. (2020) and Gómez Alba et al. (2020). The seismicity is driven by WWD in the Quifa and Rubiales oil fields in the Llanos Basin, central Colombia. Small amounts of production from these fields, which are adjacent to each other, took place in the early 1990s, but production increased significantly in 2009. The fields generate large volumes of co-produced water, which is re-injected into the flanks of the reservoir at depths of between 0.5 – 1 km. The first event in this sequence was recorded in 2012, with a significant increase in seismicity rates occurring from April 2013. Detailed event locations generated by a dedicated monitoring network (the data from which is proprietary) show two distinct clusters of events centred on the re-injection sites for each of the Quifa and Rubiales fields (Molina et al., 2020). Levels of seismicity increased from 2013 through to the occurrence of an M 4.8 event in 2015, before reducing from 2016 onwards. However, levels of seismicity increased again in 2020, leading to an M 5.0 event in March 2021. Injection and seismicity at the site has continued until the present day. The catalog we use in this study is drawn from the Servicio Geológo Colombiano catalog (https://www.sgc.gov.co/sismos), filtered between latitudes of 3.40 to 4.30° and longitudes of -71.85 to -71.00°. Information about injection start and stop times is drawn from the aforementioned publications.

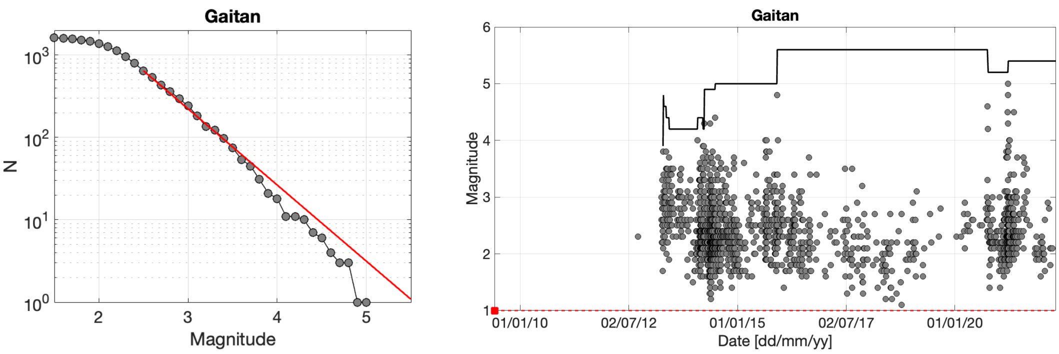

(a) *(b)*

Figure S2: Frequency-magnitude distribution and temporal evolution of magnitudes for the Puerto Gaitán sequence.

Rongchang, Sichuan, China

The seismicity generated by WWD disposal at the Rongchang gas field in the Sichuan Basin, China, has been described by Lei et al. (2008) and Wang et al. (2020). The Sichuan Basin has experienced significant levels of induced seismicity from hydraulic fracturing (e.g., Lei et al., 2019) and salt mining (e.g., Liu and Zahradník, 2020). Gas has been produced from the Rongchang field since the 1970s. WWD has taken place from the late 1970s, with fluids being injected at depths of approximately 3 km. A small amount of moderate-level seismicity was recorded through the 1980s, with levels of seismicity increasing substantially from the 1990s. The largest recorded event reached M 5.7 in August 1997. Injection in the field ceased in 2013. Despite this, seismicity has continued, with an M 4.9 event occurring in December 2016. The catalog we use in this study is that provided in the supplementary material of Wang et al. (2020), and the dates of injection start and stop are also drawn from this study.

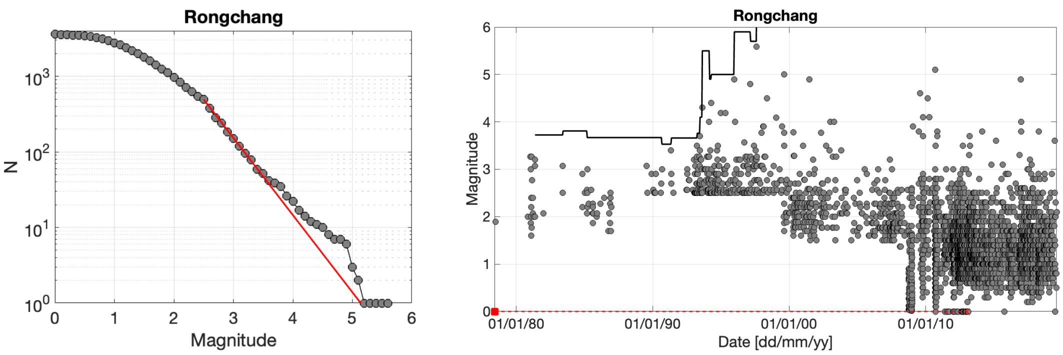

(a) *(b)*

Figure S3: Frequency-magnitude distribution and temporal evolution of magnitudes for the Rongchang sequence.

Hutubi, Xinjiang, China

The seismicity generated by NGS in the Hutubi field, Xinjiang, has been described by Tang et al. (2018); Zhou et al. (2019); and Jiang et al. (2021). The Hutubi field was originally a natural gas field. Production began in 1998 and ceased in 2009. In June 2013, the field re-started operations as an NGS facility, the largest such in China. The site operates with annual cycles of gas injection during summer months, and recovery during winter months. The gas is stored in a reservoir at a depth of approximately 3,500 m. Shortly after the onset of injection, a sequence of events was recorded in August 2013, with the largest event reaching M 3.6. This sequence ended when the field switched to extraction in October 2013. A second sequence of seismicity, with lower magnitudes (M < 3.0) began when injection restarted in the field in April 2014. Minimal seismicity was associated with the third phase of injection in summer 2015, or any subsequent phases. The catalog we use in this study is that provided in the supplementary material of Tang et al. (2018), and the dates of injection start and stop are also drawn from this study.

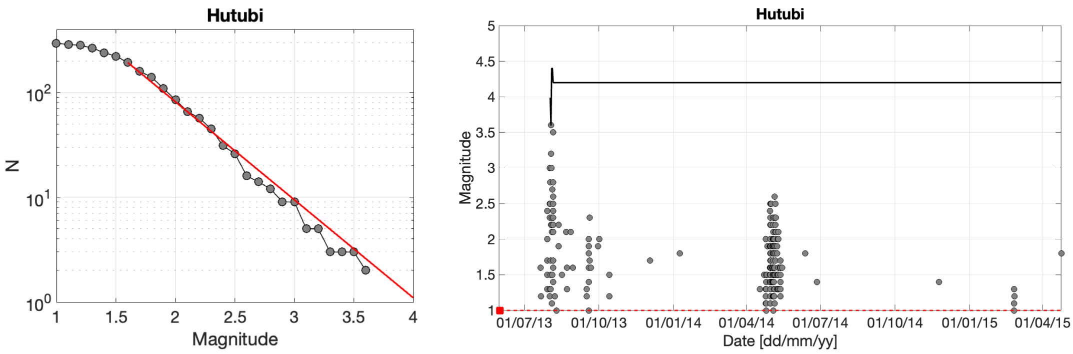

(a) *(b)*

Figure S4: Frequency-magnitude distribution and temporal evolution of magnitudes for the Hutubi sequence.

Cordel, WCSB

The seismicity induced by WWD in the Cordel oil field, Alberta is described by Schultz et al. (2014) and Verdon and Bommer (2021b). The Cordel disposal well has operated since October 1991, and has injected over 10^6 m^3 at a depth of 3,800 m into the Rundle Group. The field lies within the Cordilleran fold-and-thrust belt associated with the Laramide orogeny. A single event was recorded in July 1992, followed by a significant increase in seismicity in the late 1990s, associated with an increase in injection rates at this time.

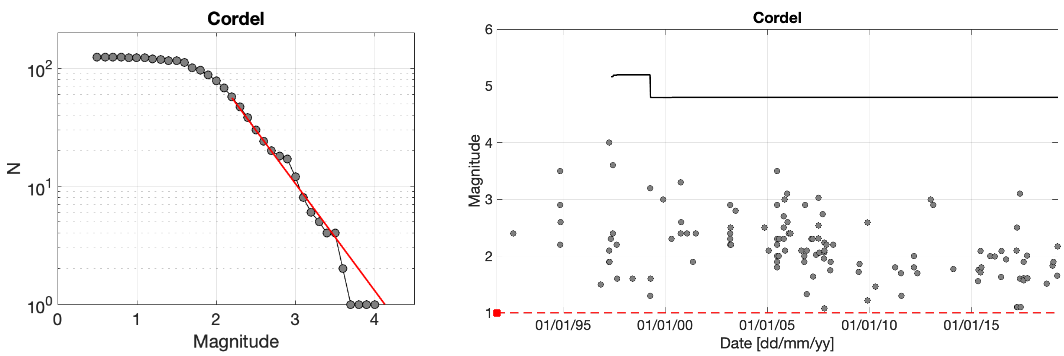

(a) *(b)*

Figure S5: Frequency-magnitude distribution and temporal evolution of magnitudes for the Cordel sequence.

The largest event, with a magnitude of M 4.0, occurred in March 1997. Injection and seismicity has continued at the Cordel field until the present. The catalog we use in this study is derived from the Composite Alberta Seismicity Catalog (CASC) (Fereidoni and Cui, 2015), filtered between latitudes of 52.50 to 52.90°, and longitudes of -116.35 to -115.95°. The injection start time for the causative well identified by Schultz et al. (2014) is sourced from the Alberta Energy Regulator (AER) Geologic Data Centre.

Eagle West, WCSB

The seismicity induced by WWD in the Eagle West oil field, near Fort St. John, British Columbia, is described by Horner et al. (1994). The Eagle West field is found within the Peace River arch in northeastern B.C.. Oil wells were drilled in the area in the 1970s, and from the early 1980s, a series of at least 7 WWD wells were drilled to re-inject produced fluids into the Permian Belloy formation at depths of around 2 km. A well-defined cluster of events can be observed (Figure S6c) centred on the locations of three high-volume wells that began injection in December 1980.

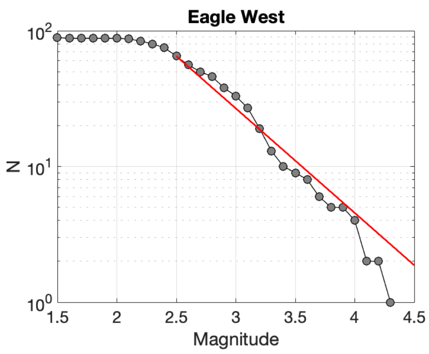

(a)

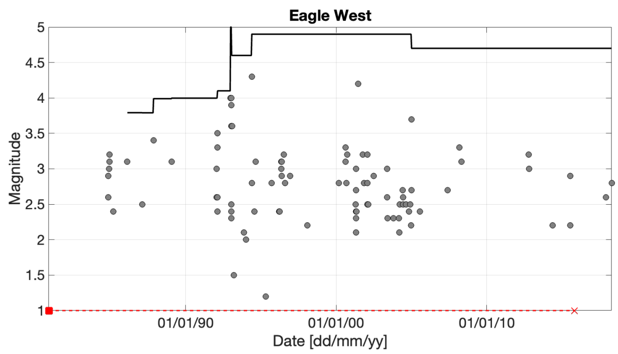

(b)

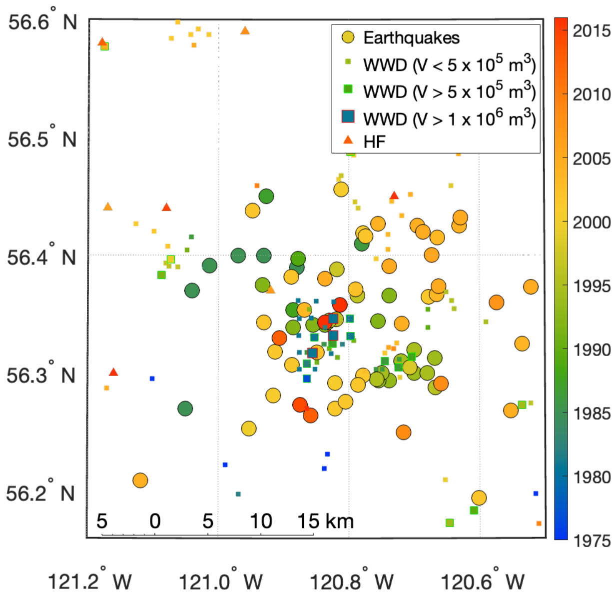

(c)

Figure S6: Frequency-magnitude distribution and temporal evolution of magnitudes for the Eagle West sequence. In (c) we show a map of earthquake locations (circles) and wells (squares = WWD wells, sized by total injected volume, triangles are HF wells). Earthquakes are coloured by their occurrence date, and wells are coloured by the date that injection began. We reprise this figure format for maps in subsequent figures.

The first seismicity in this area was observed in 1984, with magnitudes increasing over the following decade to an M 4.3 event in May 1994. The three high-volume wells ceased injection in 2015, but moderate-volume wells have continued injection in the area until the present. The catalog we use in this study is derived from the CASC, filtered between latitudes of 56.16 to 56.60°, and longitudes of -121.20 to -120.50°. Injection data is sourced from the Alberta Energy Regulator (AER) Geologic Data Centre, and we take as our injection start and end times the earliest and latest dates of injection in the three high-volume Belloy WWD wells in the centre of the event cluster.

Graham, WCSB

The seismicity induced by WWD in the Graham oil field, B.C., is described by BCOGC (2014) and Hosseini and Eaton (2018). The Graham WWD well is a former gas producer which was converted into a disposal well in January 2002. The well targets the Debolt Formation at depths of approximately 2.5 km. Seismicity around the well was first observed in November 2003, increasing in magnitude until the occurrence of an M 4.0 event in September 2010 (Figure S7c). Seismicity in this area has continued until the present.

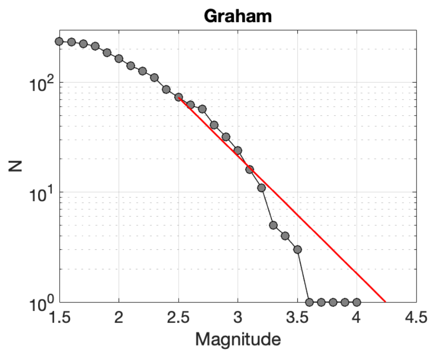

(a)

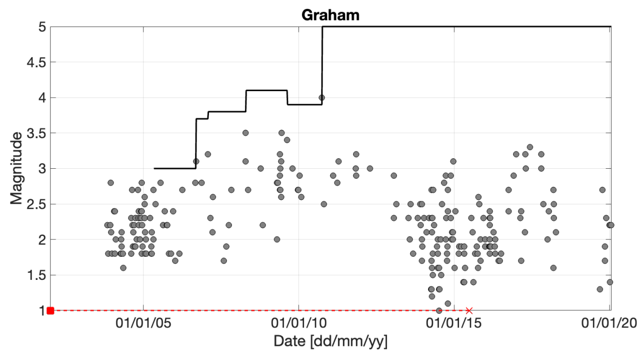

(b)

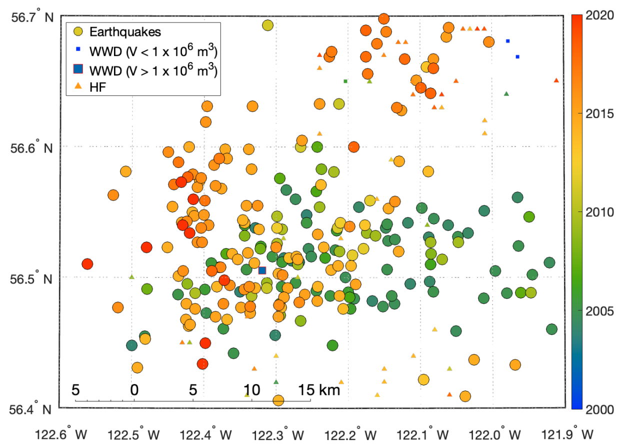

(c)

Figure S7: Frequency-magnitude distribution, temporal evolution of magnitudes, and location map for the Graham sequence. Some of the later events coincide spatially and temporally with HF wells (triangles) targeting the Montney formation, and are likely induced by hydraulic fracturing.

The Graham WWD well ceased injection in June 2015, although small-volume disposal wells in the area have continued injection. Moreover, hydraulic fracturing of the Montney Formation has also been carried out in this area, with the majority of such wells (75 %) being stimulated since 2014. Many of the events from 2014 onwards show spatial and temporal coincidence with the HF wells, indicating that multiple processes are driving induced seismicity in this region. Distinguishing between HF and WWD induced seismicity in the WCSB is not trivial (Verdon and Bommer, 2021b). The catalog we use in this study is derived from the CASC, filtered between latitudes of 56.40 to 56.70°, and longitudes of -121.60 to -120.90°. Injection data is sourced from the Alberta Energy Regulator (AER) Geologic Data Centre, and we take as our injection start and end times the earliest and latest dates of injection in the high-volume Debolt WWD well in the centre of the event cluster.

Musreau, WCSB

The seismicity induced by WWD near Musreau Lake, Alberta is described by Li et al. (2022). Musreau Lake lies approximately 80 km to the east of Crooked Lake, which has been the focus of HF-induced seismicity associated with stimulation of the Duvernay Formation. The Musreau Lake area has seen extensive hydraulic fracturing, primarily within the Montney Formation, but also targeting shallower Cretaceous-age strata such as the Dunvegan. However, there is no obvious spatial or temporal coincidence between HF wells and seismicity in this area. Since April 2017, significant volumes of flowback fluid from Montney production has been re-injected via four wells into the Devonian-age Winterburn Formation at depths of over 4 km. The onset of seismicity in proximity to these wells was observed in January 2018, with rates increasing in 2019 and culminating in an M 4.0 event in December 2019. Injection in these wells has continued until the present, as has the associated seismicity. The catalog we use in this study is that provided in the supplementary material of Li et al. (2022). Injection data is sourced from the Alberta Energy Regulator (AER) Geologic Data Centre, and we take as our injection start time the earliest date of injection in the two high-volume ($>1 \times 10^6$ m^3) Winterburn WWD wells in the centre of the event cluster.

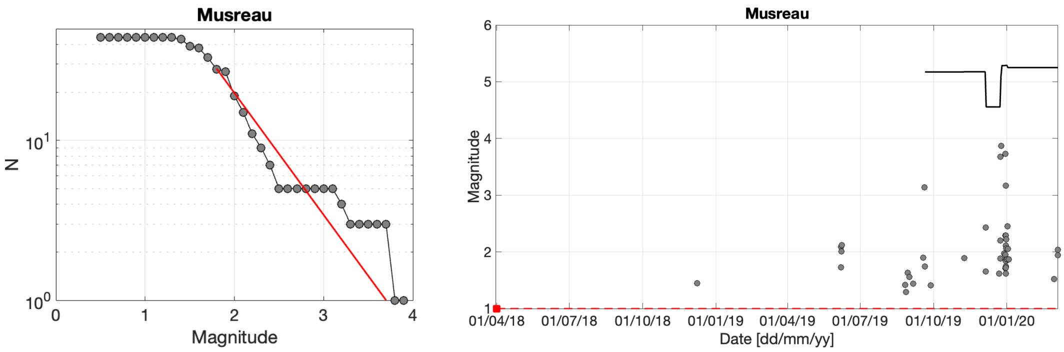

(a) *(b)*

Figure S8: Frequency-magnitude distribution and temporal evolution of magnitudes for the Musreau sequence.

Youngstown, Ohio

The seismicity induced by WWD at Youngstown, Ohio, is described by Kim (2013), Skoumal et al. (2014) and Holtkamp et al. (2015). The Northstar #1 injection well was drilled to a depth of approximately 2,700 m, into Precambrian basement rocks. The lowermost 300 m of the well was left open for injection, this interval included Cambrian sediments and the underlying basement. Injection began in late December 2010. The first felt seismicity occurred in March

2011, although subsequent analysis using matched filters (Skoumal et al., 2014) showed that the first detectable seismicity occurred on 11/01/2011, two weeks after the start of injection. Further felt seismicity, with magnitudes < 3.0, occurred during 2011, and on 30/12/2011, injection was ceased by order of the regulator. The following day, an M 4.1 event, the largest of this sequence, occurred. Subsequently, the levels of seismicity have decreased after operations stopped. The catalog we use in this study is that provided in the supplementary material of Holtkamp et al. (2015). Injection start and stop times are taken from the aforementioned papers.

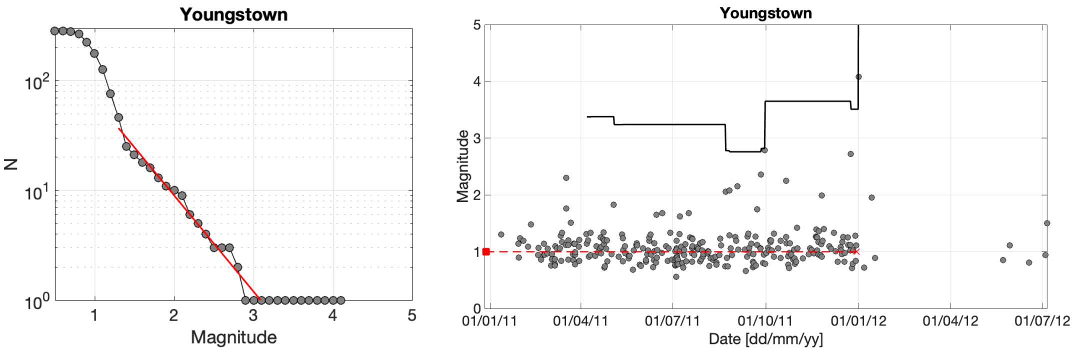

(a) *(b)*

Figure S9: Frequency-magnitude distribution and temporal evolution of magnitudes for the Youngstown sequence.

Greeley, Colorado

The Greeley WWD-induced seismicity sequence is described by Yeck et al. (2016) and Brown et al. (2017). The rate of WWD in the Denver Basin, eastern Colorado, has increased significantly over the past two decades. The Greeley site is approximately 65 km north of the Rocky Mountain Arsenal, which represents the first site at which the occurrence of WWD-induced seismicity had been recognised. On the 1st June 2014, an M 3.2 event was felt near the city of Greeley. Given the proximity of WWD wells, a possible link was suspected, and a dedicated local monitoring array was immediately installed. A number of precursory events we subsequently identified using a template matching method (Yeck et al., 2016), the first of which occurred in November 2013. This is approximately 4 months after injection began at the C4A Greeley well, in close proximity to the earthquake locations. After the M 3.2 event, the C4A well was shut in for roughly a month, and the lowermost portion of the well, which injected fluids into the Fountain Formation, directly above the Precambrian basement, was cemented, leading to a reduction in the levels of seismicity. However, in May 2015, an adjacent well, EWS-2, began injection (Brown et al., 2017), and levels of seismicity again increased until an M 2.6 event in August 2016 and an M 3.3 event in November 2016. The lower portion of EWS-2, which also targeted the Fountain Formation, was cemented after the August 2016 events. The catalog we use in this study is taken from Sheehan (2020), with additional events from the USGS Comprehensive Earthquake Catalog (ComCat), filtered between latitudes of 40.38 to 40.52°, and longitudes of -104.72 to -104.56°, appended to include earthquakes occurring before the Sheehan (2020) study. We take injection start dates from Yeck et al. (2016). Based on data from the Colorado Oil and Gas Conservation Commission, these wells have continued injection until the present day.

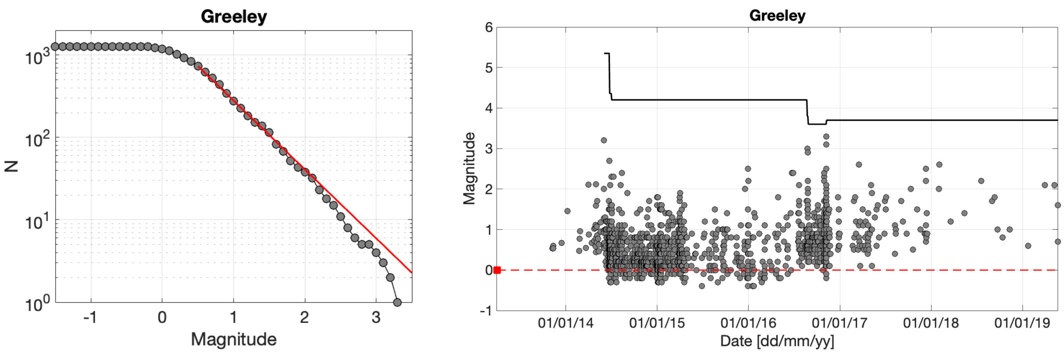

(a) *(b)*

Figure S10: Frequency-magnitude distribution and temporal evolution of magnitudes for the Greeley sequence.

Paradox Valley, Colorado

The Paradox Valley WWD-induced seismicity sequence is described by Ake et al. (2005), Block et al. (2014), and Yeck et al. (2015). In order to reduce the salinity of the Colorado River, brines from the shallow Paradox Valley aquifer are extracted, and then re-injected into deeper formations. This process isolates the brines from the near-surface hydrography. The re-injection targets basal sedimentary formations at depths of 4.3 – 4.8 km via a single disposal well. A local seismic monitoring array was installed in 1985, prior to injection tests, which ran from 1991 to 1995. Full-scale injection began in 1996. Seismicity with M < 3.0 began within 1 week of the first injection test, and continued during injection, leading to an M 4.3 event in May 2000. In response to this event, injection rates were reduced, and biannual shut-down periods were introduced. This led to a reduction in seismicity rates. However, since the mid-2000s, injection pressures have gradually risen (Block et al., 2014), leading to a further increase in seismicity, and in 2013 a further M 4.4 event occurred, followed by an M 4.5 event in March 2019. The catalog we use in this study is provided by the National Energy Technology Laboratory (NETL) (https://edx.netl.doe.gov/dataset/paradox-valley-seismic-and-injection-data), which runs until 2014, with additional events from the USGS ComCat database, filtered between latitudes of 38.10 to 38.45°, and longitudes of -109.40 to -108.50°, from 2014 to the present. We take injection start dates from Ake et al. (2005), and we assume that injection has continued until the present day.

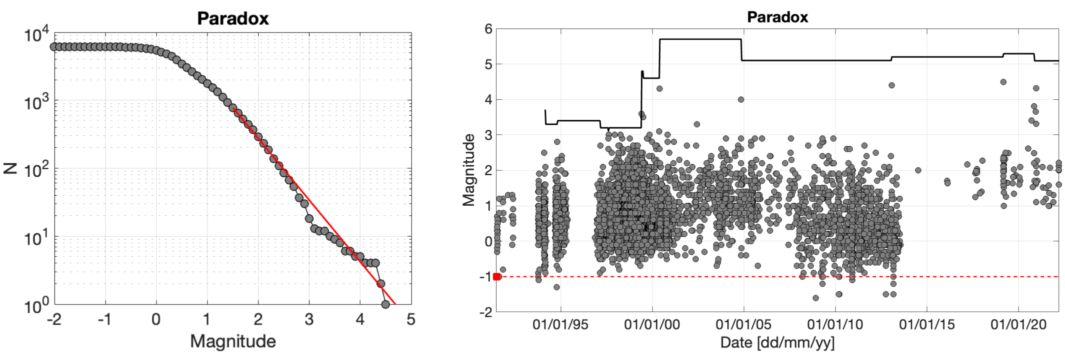

(a) *(b)*

Figure S11: Frequency-magnitude distribution and temporal evolution of magnitudes for the Paradox Valley sequence.

Raton Basin, Colorado/New Mexico

The Raton Basin WWD-induced seismicity sequence is described by Meremonte et al. (2002), Rubenstein et al. (2014), Nakai et al. (2017), and Glasgow et al. (2021). In the Raton Basin, wastewater associated with coal-bed methane production has been injected via over 20 wells into the Dakota Formation, at depths of 1,250 to 2,100 m. Injection began in 1994 and increased substantially in the late 1990s/early 2000s (Rubinstein et al., 2014). The first M > 3.0 events were detected in 1995, and the first widely-reported seismicity was the M 4.5 event in September 2001. Further sequences included an M 5.0 event in August 2005, and an M 5.3 event in August 2011. Since 2011, the monthly injected volume has decreased (Glasgow et al., 2021) as has the level of seismicity, although an M 4.0 event occurred in November 2021. The catalog we use in this study is derived from the USGS ComCat, filtered between latitudes of 36.20 to 37.80°, and longitudes of -105.40 to -103.80°. We take injection start dates from Rubinstein et al. (2014), and we assume that injection has continued until the present day.

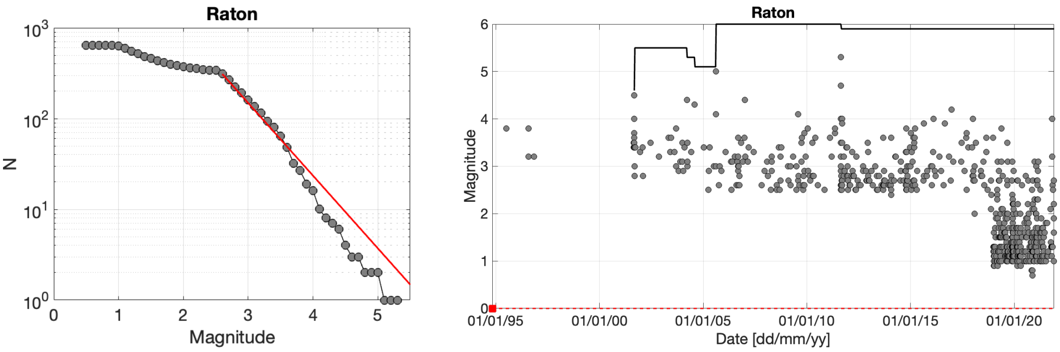

(a) *(b)*

Figure S12: Frequency-magnitude distribution and temporal evolution of magnitudes for the Raton Basin sequence.

Guy-Greenbrier, Arkansas

The Guy-Greenbrier WWD-induced seismicity sequence is described by Horton (2012), Ogwari et al. (2016), and Yoon et al. (2017). As hydraulic fracturing of the Fayetteville Shale has developed in Arkansas, flowback and produced fluids have been re-injected into deep formations. From April 2009 in an area between the cities of Guy and Greenbrier, WWD was initiated via several wells into the Springfield and Ozark aquifers at depths from 1.7 to 3.3 km. Hydraulic fracturing of the Fayetteville Shale was also taking place in this area. From late 2009 onwards, a significant increase in seismicity was observed along a NE-SW trending-structure, now termed the Guy-Greenbrier fault (Horton, 2012). The onset of seismicity along this structure followed the onset of WWD in several adjacent wells. Additionally, some seismicity around this main Guy-Greenbrier structure than can be clearly attributed to HF activities (Yoon et al., 2017). Elevated rates of seismicity continued until 2011, with the largest event reaching M 4.7 in February 2011. The WWD wells thought to be responsible for the seismicity had all ceased injection by mid-2011, after which the levels of seismicity decreased substantially over the following few months. The catalog we use in this study is derived from the USGS ComCat, filtered between latitudes of 35.10 to 35.50°, and longitudes of -92.60 to -92.10°. Some of the events within this area show a clear link to HF activities (Yoon et al., 2017), so we further refine our event catalog, choosing only events within the polygon shown in Figure S12c, which corresponds to the events primarily driven by WWD. Injection start and stop times are taken from Horton (2012).

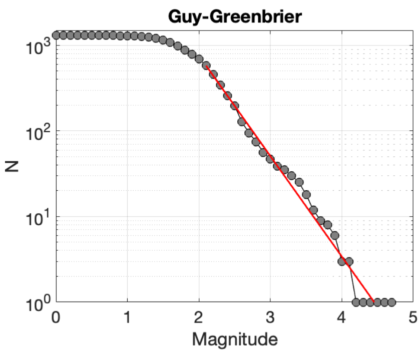

(a)

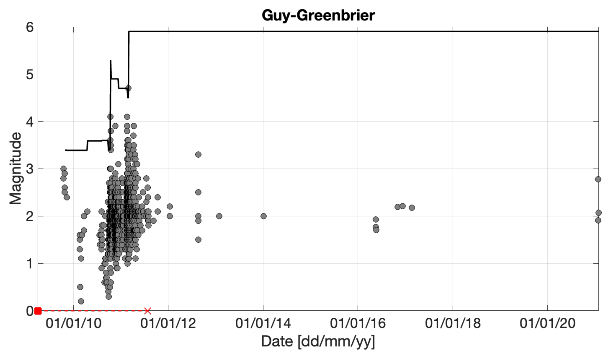

(b)

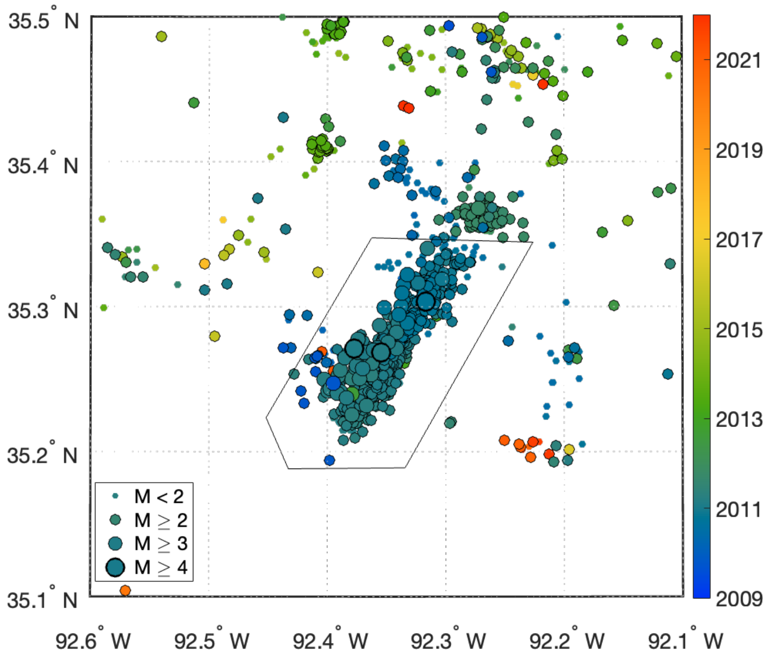

(c)

Figure S13: Frequency-magnitude distribution, temporal evolution of magnitudes, and event location map for the Guy-Greenbrier sequence. In (c), the black polygon delineates events driven primarily by WWD along the Guy-Greenbrier fault, which we select for our analysis.

Oklahoma and southern Kansas: Cushing, Fairview, Guthrie-Langston, Pawnee, Prague, Milan, Harper

The upsurge in seismicity in Oklahoma since 2010 represents one of the most prominent and significant examples of WWD-induced seismicity worldwide, and it has been the subject of extensive study. From the early 2000s, volumes of wastewater injection steadily increased from less than 1×10^6 m^3 to c. 4×10^6 m^3 per month (Langenbruch and Zoback, 2016). This injection was dominated by produced water from conventional fields, with some contribution from HF flowback fluids (Rubinstein and Mahani, 2015). From the early 2010s, the volumes of wastewater injection increased substantially to over 12×10^6 m^3 per month. The primary target for WWD is the Arbuckle Formation, which sits directly above the Precambrian basement.

This increase in WWD volumes was accompanied by a significant increase in rates of seismicity, with the locus of seismicity tracking the development of injection wells. At the northern boundary of Oklahoma, seismicity has extended into the southern portion of Kansas.

The objective of our study is to examine the temporal evolution of induced event magnitudes within a given sequence. Within this context, the seismicity in Oklahoma and southern Kansas could potentially be treated as a single sequence. However, given the richness of data available from this region, our preferred approach is to identify individual cases where a clear, spatially delimited sequence can be identified. We also focus on cases where large-magnitude events were induced. The sequences we use in our study are Prague (Keranen et al., 2013); Guthrie-Langston (Schoenball et al., 2018); Cushing (McGarr and Barbour, 2017); Pawnee (Walter et al., 2017); and Fairview (Goebel et al., 2017); and the Milan and Harper sequences from Kansas (Verdecchia et al., 2021). For the Oklahoma sequences, we source event catalogs from the Oklahoma Geological Survey (Walter et al., 2020), while for the Kansas sequences we use the USGS ComCat database. For Oklahoma we source injection well data from the Oklahoma Corporation Commission (OCC).

Figure S14c shows a map of event locations and injection wells for the Cushing sequence. We select events between latitudes of 35.90 < Lat < 36.09° and longitudes between -96.92 < Lon < -96.70°. We identify 7 high-volume ($> 5 \times 10^5$ m^3) injection wells within the vicinity of the sequence. The earliest injection in these wells took place in February 2011, and injection via some of these wells has continued until the end of 2021 (the latest available data in the OCC database).

Figure S15c shows a map of event locations and injection wells for the Fairview sequence. We select events between 36.20 < Lat < 36.80° and -99.20 < Lon < -98.20°. We identify numerous high-volume ($> 5 \times 10^5$ m^3) injection wells within the vicinity of the sequence, the nearest of which injected over 1.5×10^6 m^3 before the first detect event. Injection in this well began prior to 2006 (the earliest available data in the OCC database) and injection via some of these wells has continued until the end of 2021 (the latest available data in the OCC database).

Figure S16c shows a map of event locations and injection wells for the Guthrie-Langston sequence. We select events between 35.70 < Lat < 36.00° and -97.70 < Lon < -97.10°. We identify numerous high-volume ($> 5 \times 10^5$ m^3) injection wells within the vicinity of the sequence, many of which began injection prior to 2006 (the earliest available data in the OCC database). Injection via some of these wells has continued until the end of 2021 (the latest available data in the OCC database).

Figure S17c shows a map of event locations and injection wells for the Pawnee sequence. We select events between 36.32 < Lat < 36.52° and -97.00 < Lon < -96.70°. Numerous high-volume ($> 5 \times 10^5$ m^3) injection wells are located within the vicinity of the sequence. Keranen et al. (2013) reports injection taking place in at least one of these wells from 1993 onwards. Injection via some of these wells has continued until the end of 2021 (the latest available data in the OCC database).

For the Kansas sequences we use the USGS ComCat database, filtered between 37.20 < Lat < 37.31° and -98.02 < Lon < -97.92° for the Harper sequence, and 37.20 < Lat < 37.35° and -97.70 < Lon < -97.55° for the Milan sequence. We adopt injection start times from the data plotted in Figure 8 of Verdecchia et al. (2021) and assume that injection has continued to the present day.

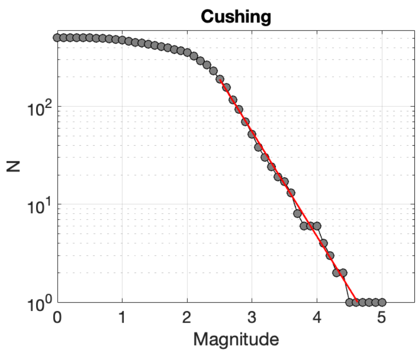

(a)

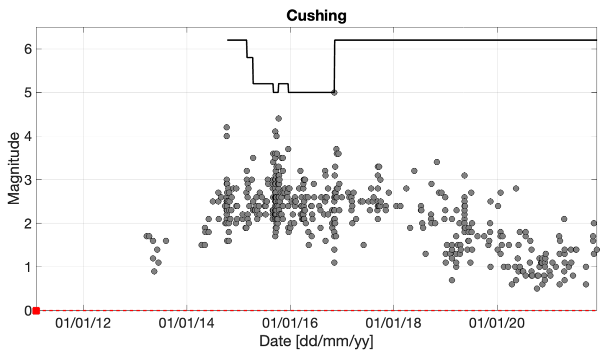

(b)

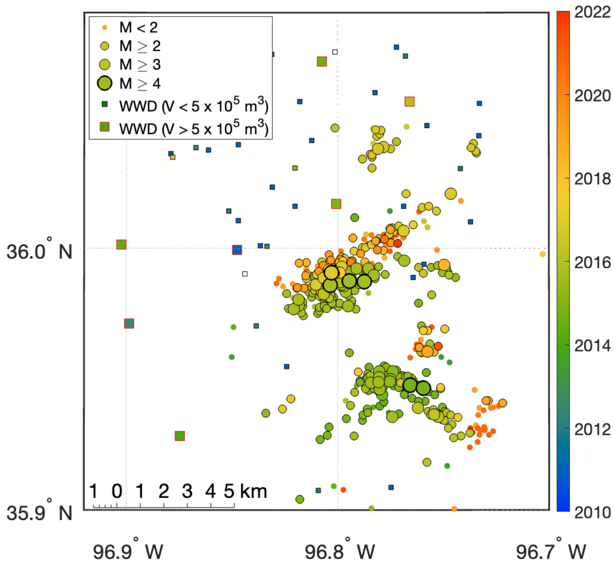

(c)

Figure S14: Frequency-magnitude distribution, temporal evolution of magnitudes, and event location map for the Cushing sequence.

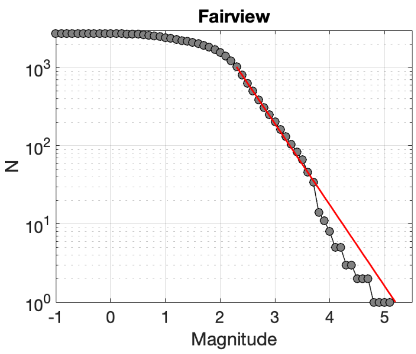

(a)

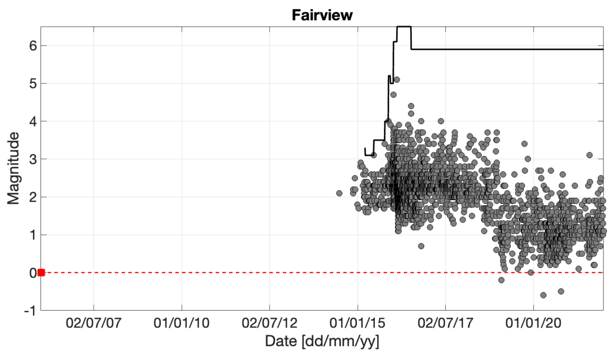

(b)

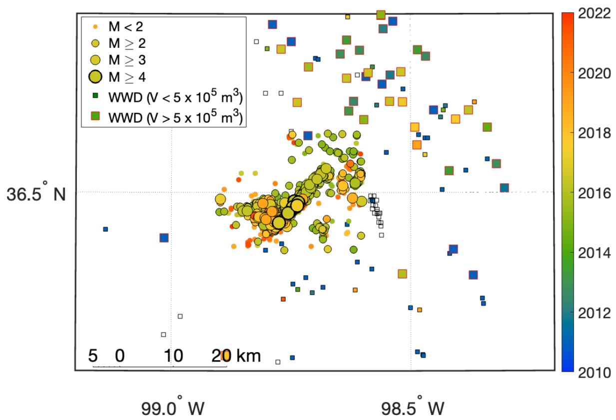

(c)

Figure S15: Frequency-magnitude distribution, temporal evolution of magnitudes, and event location map for the Fairview sequence.

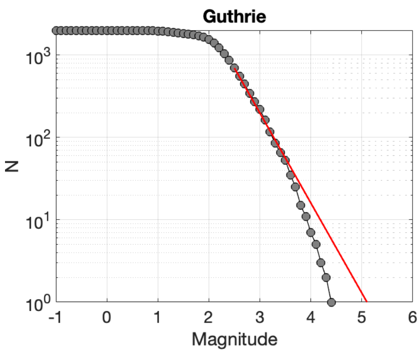

(a)

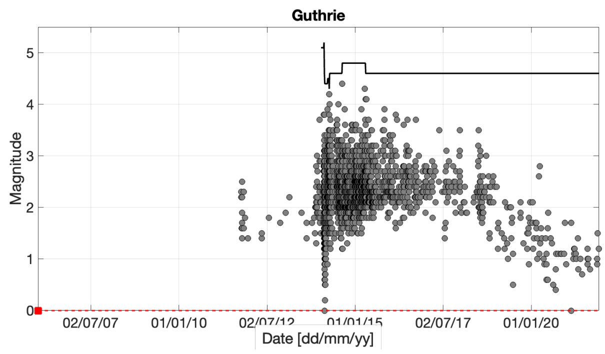

(b)

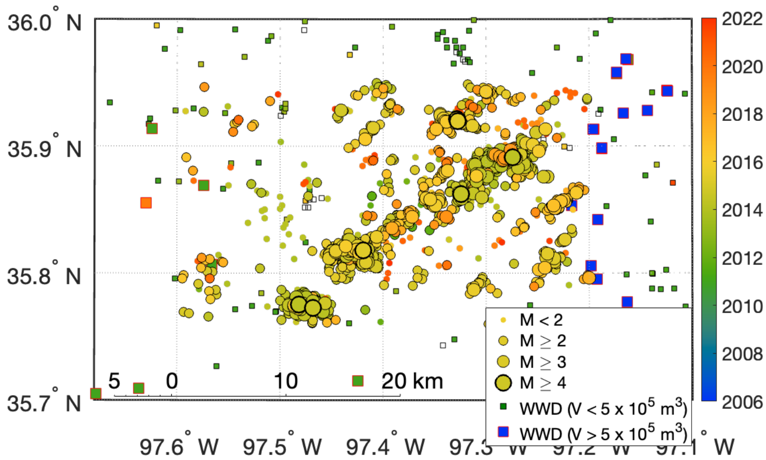

(c)

Figure S16: Frequency-magnitude distribution, temporal evolution of magnitudes, and event location map for the Guthrie-Langston sequence.

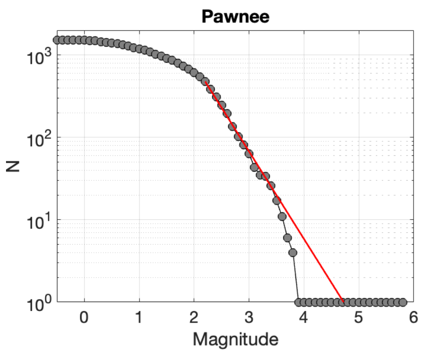

(a)

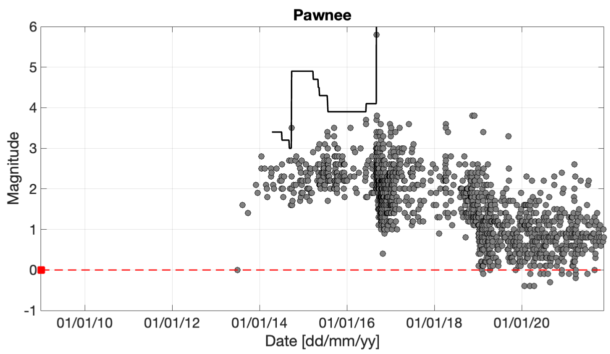

(b)

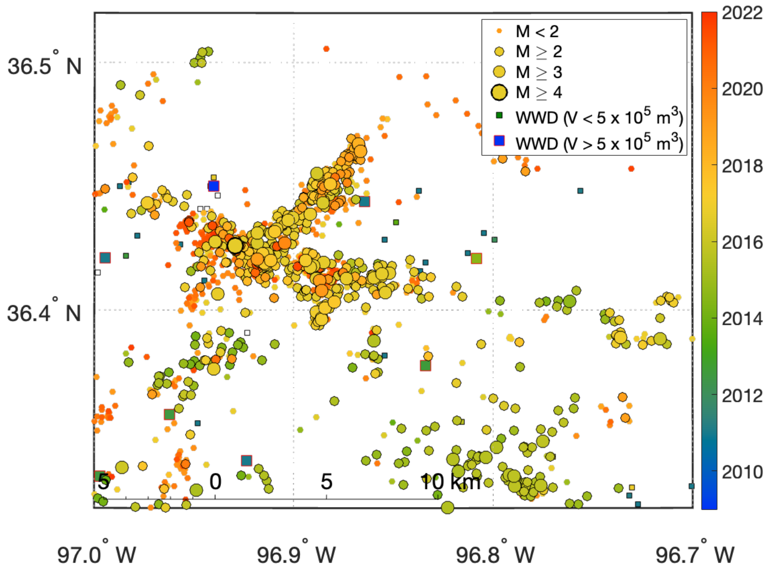

(c)

Figure S17: Frequency-magnitude distribution, temporal evolution of magnitudes, and event location map for the Pawnee sequence.

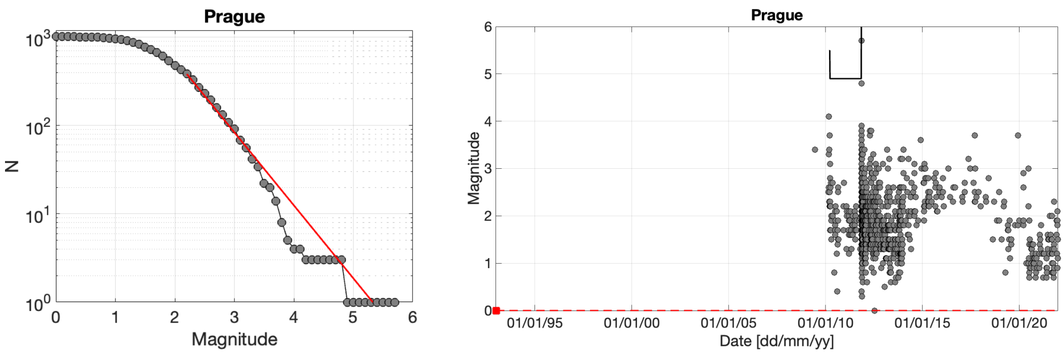

(a) (b)

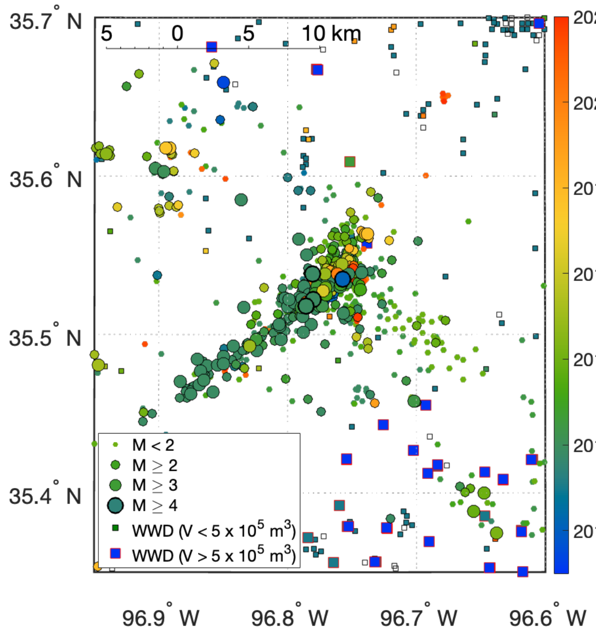

(c)

Figure S18: Frequency-magnitude distribution, temporal evolution of magnitudes, and event location map for the Prague sequence.

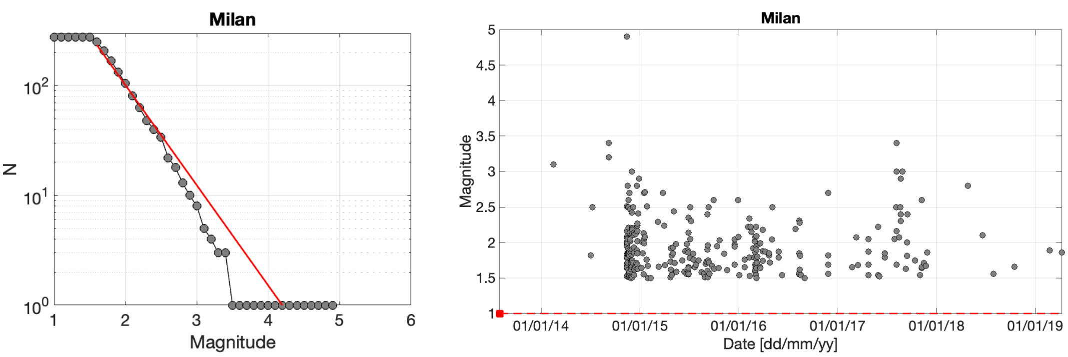

(a) (b)

Figure S19: Frequency-magnitude distribution and temporal evolution of magnitudes for the Milan sequence.

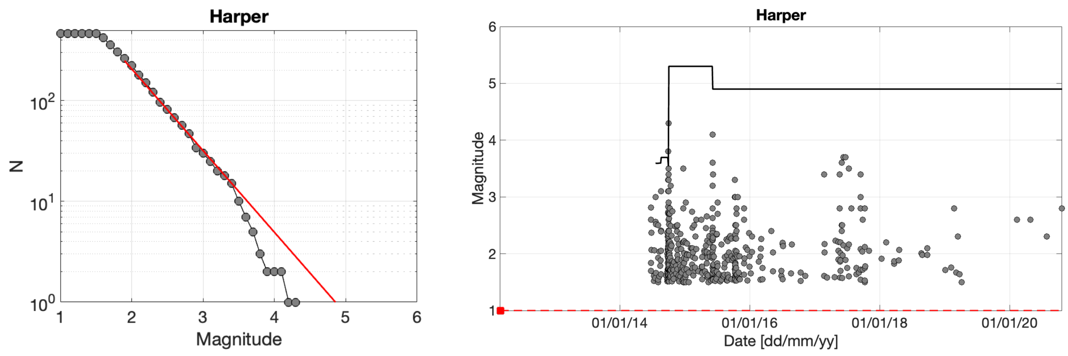

(a) *(b)*

Figure S20: Frequency-magnitude distribution and temporal evolution of magnitudes for the Harper sequence.

Fort Worth Basin: Azle-Reno, Dallas, Irving, Venus

Alongside the increase in induced seismicity observed in Oklahoma, similar behaviour has been observed in the Fort Worth Basin, East Texas, with a significant increase in WWD into deep aquifers being associated with numerous sequences of induced seismicity (Frohlich, 2012; Hennings et al., 2021). Prior to 2008, no earthquakes had been detected in this region. The Ellenburger Formation, which sits directly above the crystalline basement, is the primary target for WWD.

Using USArray data, Frohlich (2012) identified approximately 100 earthquakes within the Fort Worth Basin, the majority of which were spatially associated with high-volume injection wells. These clusters were further studied by Hennings et al. (2021), who combined existing catalogs with template matching to produce a comprehensive catalog for the Fort Worth Basin. Hennings et al. (2021) identified 10 discrete clustered sequences of which four, Azle-Reno, Dallas-Fort Worth, Irving, and Venus produced M > 3.0 events. The catalogs we use in this study are taken from the supplementary material of Hennings et al. (2021). Injection well data is sourced from the supplementary material of Gao et al. (2021).

Figure S21c shows a map of event locations and injection wells for the Azle-Reno sequence. A single high-volume injection well is adjacent to the sequence. The earliest injection in this well took place in June 2009, and has continued until the present. Figure S22c shows a map of event locations and injection wells for the Azle-Reno sequence. A single high-volume injection well is adjacent to the sequence. The earliest injection in this well took place in September 2008, and the well ceased injection in August 2009. Figure S23c shows a map of event locations and injection wells for the Irving sequence. Two high-volume injection wells are located approximately 10 km from the sequence. One of these began injection in September 2008 and ceased injection in August 2009, and the other begain injection November 2007 and has continued until the present. Figure S24c shows a map of event locations and injection wells for the Venus sequence. Five high-volume injection wells are located around the event cluster. The earliest injection in one of these wells took place in October 2006, and injection has continued in three of the wells until the present.

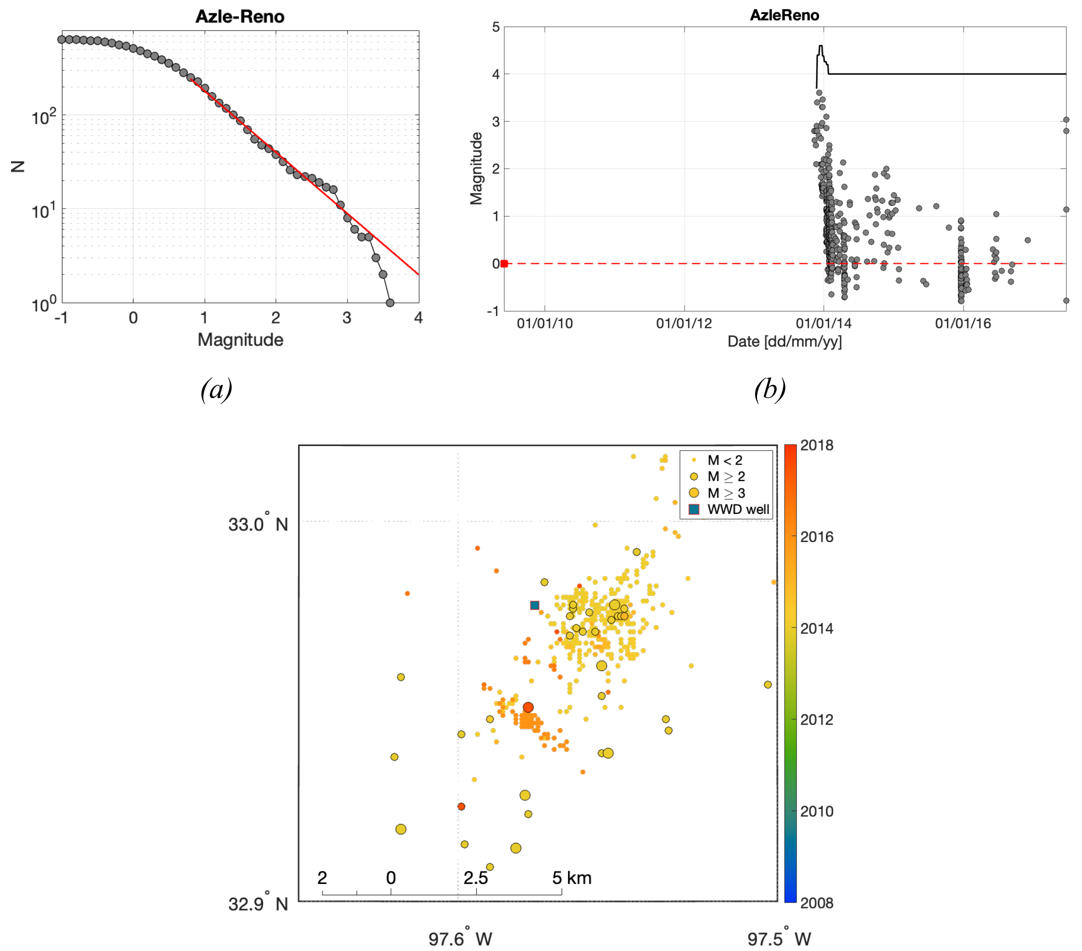

(a) *(b)*

(c)

Figure S21: Frequency-magnitude distribution, temporal evolution of magnitudes, and event location map for the Azle-Reno sequence.

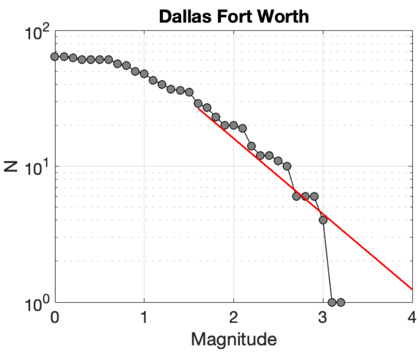

(a)

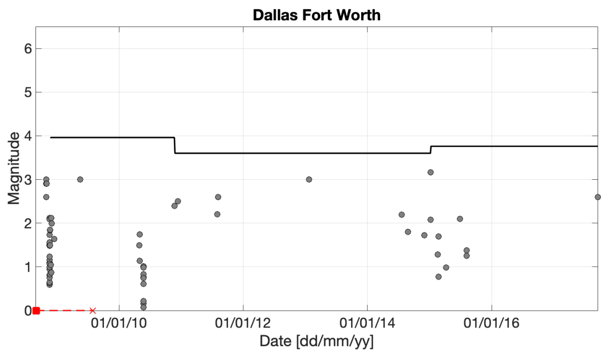

(b)

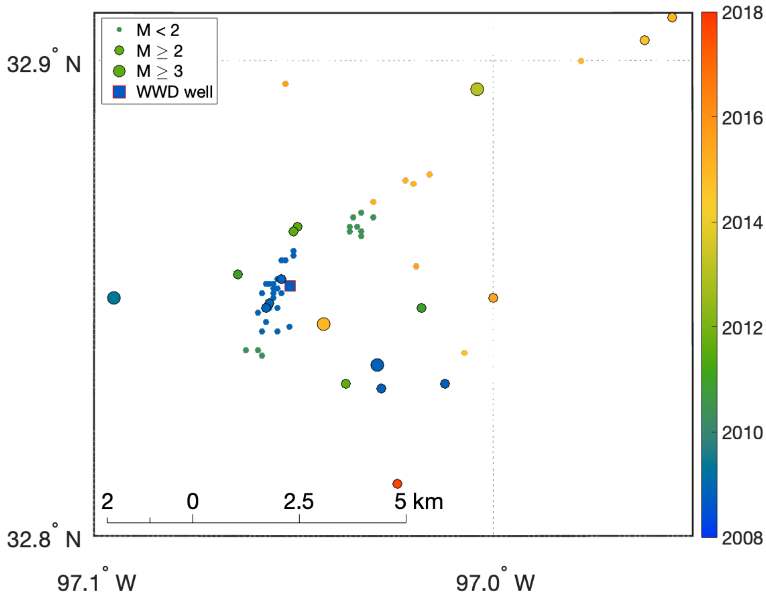

(c)

Figure S22: Frequency-magnitude distribution, temporal evolution of magnitudes, and event location map for the Dallas Fort Worth sequence.

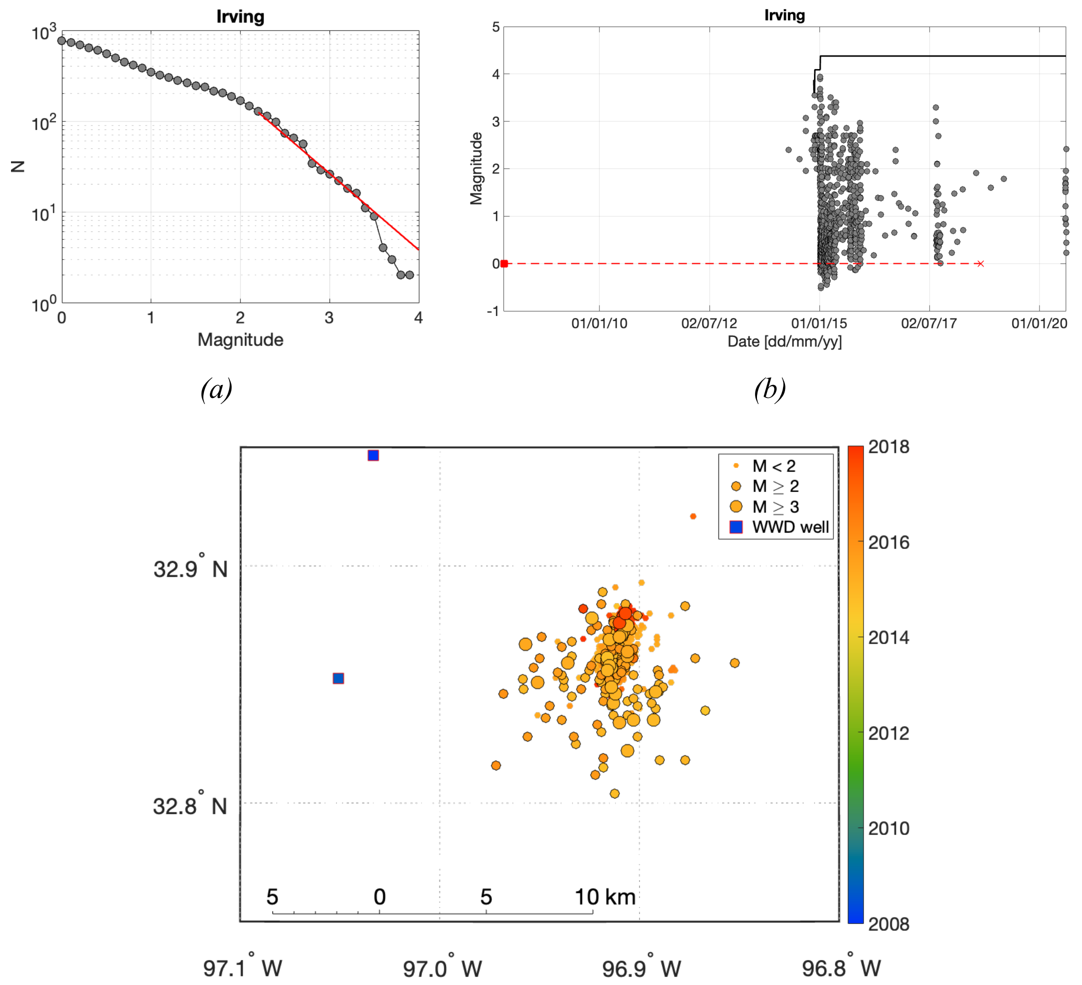

(c)

Figure S23: Frequency-magnitude distribution, temporal evolution of magnitudes, and event location map for the Irving sequence.

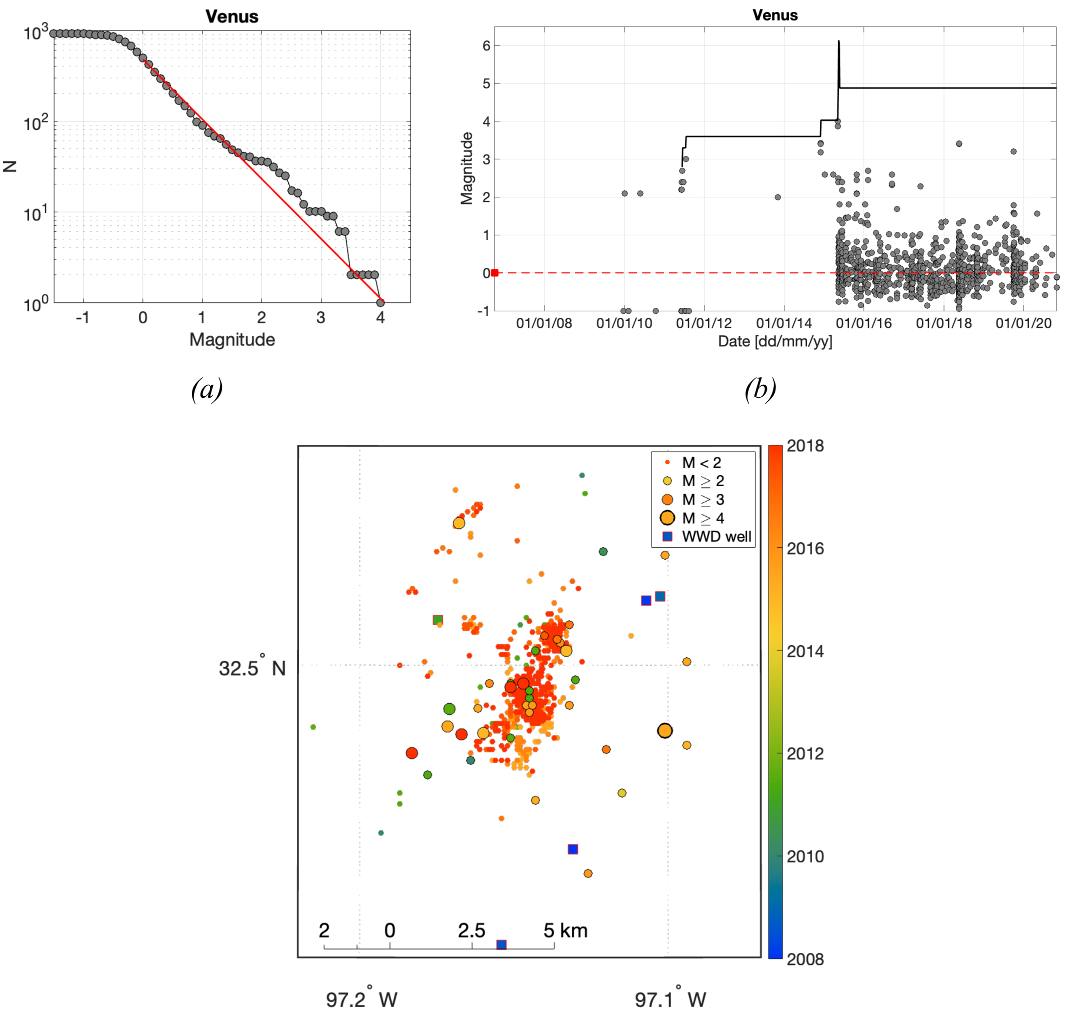

(a) *(b)*

(c)

Figure S24: Frequency-magnitude distribution, temporal evolution of magnitudes, and event location map for the Venus sequence.

Timpson, East Texas

To the east of the Fort Worth Basin, the Timpson sequence is described by Frohlich et al. (2014), Fan et al. (2016) and Wang et al. (2020). Two high-volume WWD wells began injection in 2006 and 2007. Unlike most induced seismicity in the mid-continental USA, the wells targeted relatively shallow depths, at 1.8 – 1.9 km, whereas the crystalline basement is at 5 km depth. The first seismicity in this area was recorded in 2008, although levels of seismicity remained relatively low until the occurrence of an M 4.8 event in May 2012, followed by a series of aftershocks continuing through 2013. Injection volumes were reduced significantly in late 2013. No seismicity was recorded in the area from 2014 until a further series of events, with a maximum magnitude of M 4.3, began in 2018. The catalogs we use in this study are taken from the supplementary material of Frohlich et al. (2014), with additional events taken from the USGS ComCat database, filtered between latitudes of 31.70 to 32.00°, and longitudes of -94.50 to -94.30°. We sourced injection data from the Texas Railroad Commission (https://www.rrc.texas.gov).

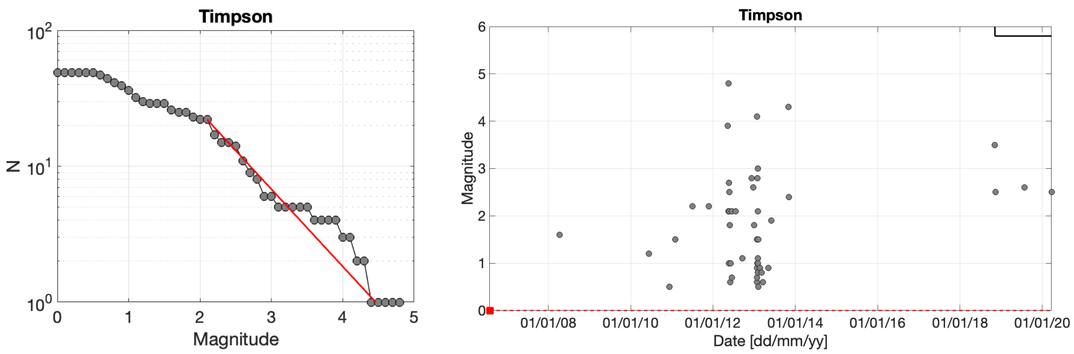

(a) *(b)*

Figure S25: Frequency-magnitude distribution and temporal evolution of magnitudes for the Timpson sequence.

Cogdell, Texas

The seismicity induced by gas injection at the Cogdell oilfield in northern Texas is described by Gan and Frohlich (2013). The Cogdell field was discovered in the late 1940s, and from 1956 to 1982, water injection was used for secondary recovery. In the late 1970s, a series of 17 earthquakes were detected, with a maximum magnitude of M = 4.6, associated with this wastewater disposal (Davis and Pennington, 1989). Due to the lack of an available catalog, and the paucity of event detection, we do not consider the 1970s sequence in our analysis. Secondary recovery under waterflooding continued until the early 2000s. In 2001, the use of CO_2 injection to enhance recovery was initiated in the Cogdell field.

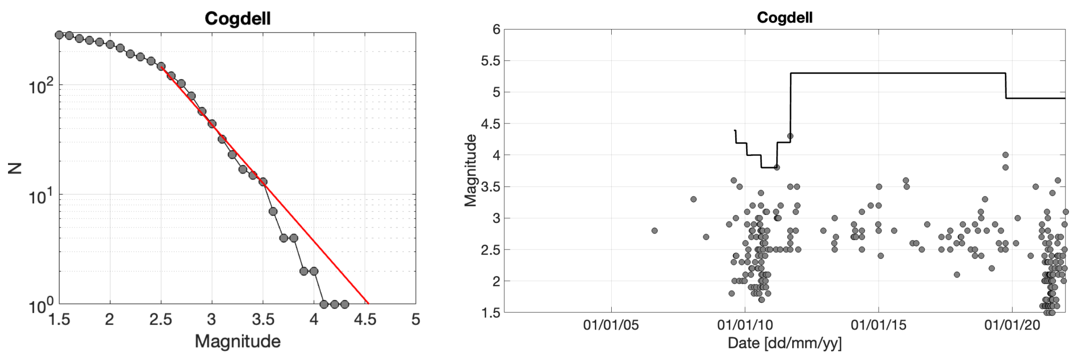

(a) *(b)*

Figure S26: Frequency-magnitude distribution and temporal evolution of magnitudes for the Cogdell sequence.

After the onset of CO_2 injection, further seismicity was observed, starting in August 2006. The largest event reached M 4.3 in 2011, and seismicity has continued until the present. Gan and Frohlich (2013) used USArray data to produce a more detailed event catalog during 2010-2011, and argued that the spatial and temporal evolution of the sequence is consistent with their being induced by the CO_2 injection, especially as there has otherwise been little change in the rates of liquid (oil and water) production and reinjection, and the net liquid volume change is negative (i.e., more fluid is withdrawn than reinjected). The catalogs we use in this study are taken from the supplementary material of Gan and Frohlich (2013), with additional events taken from the USGS ComCat database, filtered between latitudes of 32.50 to 33.60°, and longitudes of -101.60 to -100.20°. Information regarding the onset of CO_2 injection is sourced from Gan and Frolich (2013), and we assume that injection has continued until the present.

Reeves, Texas

The past decade has seen a significant increase in the use of both hydraulic fracturing and high-volume WWD in the Delaware Basin of western Texas. This surge in activity has been accompanied by the development of induced seismicity, which has been associated with both wastewater disposal and hydraulic fracturing (e.g., Skoumal et al., 2020). Much like the situation in Oklahoma (described above), the density of wells and the resulting overlap in seismicity means that it can be challenging to isolate individual sequences in order to provide a detailed examination of their onset and temporal evolution relative to the wells that caused them. However, the largest event that has occurred to date, the 26/03/2020 M 4.9 event in Reeves County, roughly 50 km northwest of the city of Pecos, does appear to have occurred within an isolated sequence that can be examined in detail. Figure S27c shows a map of the earthquake sequence and nearby injection wells.

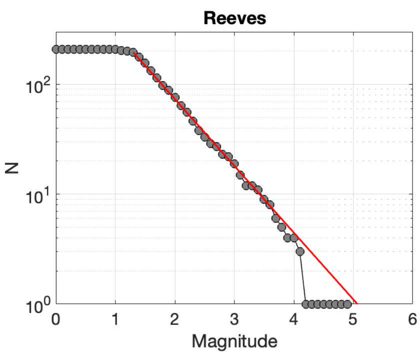

(a)

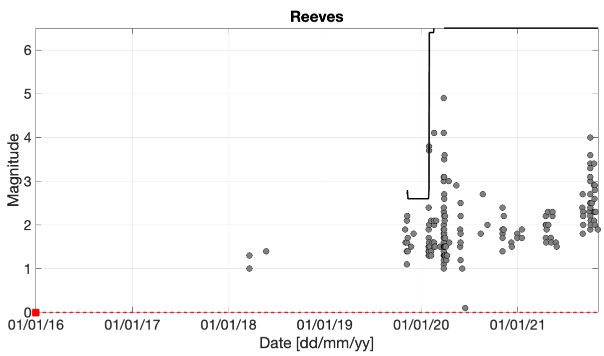

(b)

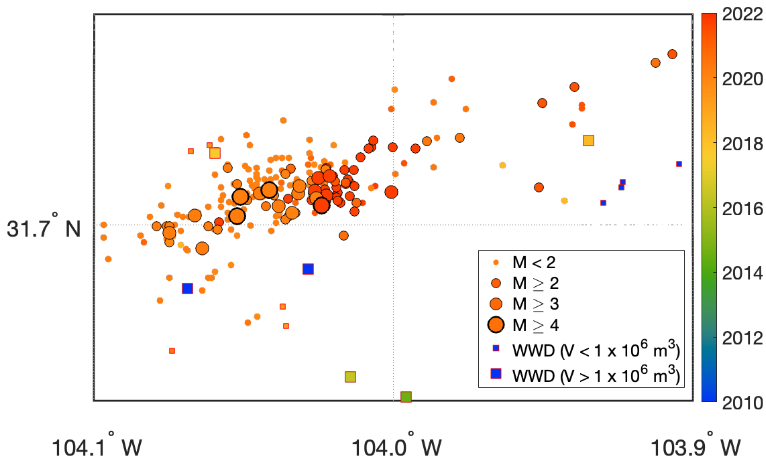

(c)

Figure S27: Frequency-magnitude distribution, temporal evolution of magnitudes, and event location map for the Reeves sequence

Injection data is sourced from the Texas Railroad Commission (https://www.rrc.texas.gov). Six high volume WWD wells are located around the earthquake swarm. Two of these wells began injection in the 1980s and had ceased injection before the onset of the seismicity. Of the remaining wells, the first injection took place in January 2016. Earthquake data is sourced from the TexNet catalog (Savvaidis et al., 2019) found at (https://www.beg.utexas.edu/texnet-cisr/texnet/earthquake-catalog), filtered between latitudes of 31.65 to 31.76°, and longitudes of -104.10 to -103.90°.

References

BCOGC, 2014. Investigation of observed seismicity in the Montney trend. B.C. Oil and Gas Commission, 32 pp. Available at: https://www.bcogc.ca/files/reports/Technical-Reports/investigation-observed-seismicity-montney-trend.pdf (last accessed 14/04/2022).

Brown, M.R.M., S. Ge, A.F. Sheehan, J.S. Nakai, 2017. Evaluating the effectiveness of induced seismicity mitigation: numerical modeling of wastewater injection near Greeley, Colorado: Journal of Geophysical Research 122, 6569-6582.

Butcher, A., R. Luckett, J.P. Verdon, J-M. Kendall, B. Baptie, J. Wookey, 2017. Local magnitude discrepancies for near-event receivers; implications for the UK traffic light scheme: Bulletin of the Seismological Society of America 107, 532-541.

Butcher, A., R. Luckett, J-M. Kendall, B. Baptie, 2020. Seismic magnitudes, corner frequencies, and microseismicity: using ambient noise to correct for high-frequency attenuation: Bulletin of the Seismological Society of America 110, 1260-1275.

Cesca, S., F. Grigoli, S. Heimann, Á. González, E. Buforn, S. Maghsoudi, E. Blanch, T. Dahm, 2014. The 2013 September-October seismic sequence offshore Spain: a case of seismicity triggered by gas injection? Geophysical Journal International 198, 941-953.

Fan, Z., P. Eichhubl, J.F.W. Gale, 2016. Geomechanical analysis of fluid injection and seismic fault slip for the M_W 4.8 Timpson, Texas, earthquake sequence: Journal of Geophysical Research 121, 2798-2812.

Fereidoni, A., and L. Cui, 2015. Composite Alberta Seismicity Catalog: CASC2014-x. Available at: https://www.inducedseismicity.ca/wp-content/uploads/2015/01/Composite-Alberta-Seismicity-Catalog3.pdf (last accessed 14/04/2022).

Gao, S., J-P. Nicot, P.H. Hennings, P. La Point, K.M. Smye, E.A. Horne, R. Dommisse, 2021. Low pressure buildup with large disposal volumes of oil field water: a flow model of the Ellenburger Group, Fort Worth Basin, northcentral Texas: AAPG Bulletin 105, 2575-2593.

Glasgow, M., B. Schmandt, R. Wang, M. Zhang, S.L. Bilek, E. Kiser, 2021. Raton Basin induced seismicity is hosted by networks of short basement faults and mimics tectonic earthquake statistics: Journal of Geophysical Research 126, e2021JB022839.

Gómez-Alba, S., C.A. Vargas, A. Zang, 2020. Evidencing the relationship between injected volume of water and maximum expected magnitude during the Puerto Gaitán (Colombia) earthquake sequence from 2013 to 2015: Geophysical Journal International 220, 335-344.

Holtkamp, S.G., M.R. Brudzinski, B.S. Currie, 2015. Regional detection and monitoring of injection-induced seismicity: application to the 2010-2012 Youngstown, Ohio, seismic sequence: AAPG Bulletin 99, 1671-1688.

Jiang, G., L. Liu, A.J. Barbourm R. Lu, H. Yang, 2021. Physics-based evaluation of the maximum magnitude of potential earthquakes induced by the Hutubi (China) underground gas storage: Journal of Geophysical Research 126, e2020JB021379.

Lei, X., G. Yu, S. Ma, X. Wen, Q. Wang, 2008. Earthquakes induced by water injection at ~3 km depth within the Rongchang gas field, Chongqing, China: Journal of Geophysical Research 113, B10310.

Liu, J. and J. Zahradník, 2020. The 2019 M_W 5.7 Changning earthquake, Sichuan Basin, China: a shallow doublet with different faulting styles: Geophysical Research Letters 47, e2019GL085408.

Meremonte, M.E., J.C. Lahr, A.D. Frankel, J.W. Dewey, A.J. Crone, D.E. Overturf, D.L. Carver, W.T. Bice, 2002. Investigation of an earthquake swarm near Trinidad, Colorado, August-October 2001: U.S. Geological Survey, Open File Report OFR-02-0073.

Ogwari, P.O., S.P. Horton, S. Ausbrooks, 2014. Characteristics of induced/triggered earthquakes during the startup phase of the Guy-Greenbrier earthquake sequence in north-central Arkansas: Seismological Research Letters 87, 620-630.

Rubinstein, J.L., W.L. Ellsworth, A. McGarr, H.M. Benz, 2014. The 2001-present induced earthquake sequence in the Raton Basin of northern New Mexico and southern Colorado: Bulletin of the Seismological Society of America 104, 2162-2181.

Ruiz-Barajas, S., N. Sharma, V. Convertito, A. Zollo, B. Benito, 2017. Temporal evolution of a seismic sequence induced by a gas injection in the Eastern coast of Spain: Nature Scientific Reports 7, 2901.

Seeber, L., and J.G. Armbruster, 1993. Natural and induced seismicity in the Lake Erie-Lake Ontario region: reactivation of ancient faults with little Neotectonic displacement: Geographie Physique et Quaternaire 47, 363-378.

Sheehan, A.F., 2020. Capturing the onset of induced seismicity: field experiment at high rate disposal wells, Denver-Julesburg Basin, Colorado: Final Technical Report for Award #G18AP00079. United States Geological Survey. Available at: https://earthquake.usgs.gov/cfusion/external_grants/reports/G18AP00079.pdf, last accessed 08/02/2023.

Verdon, J.P., and J.J. Bommer, 2021b. Comment on “Activation rate of seismicity for hydraulic fracture wells in the Western Canadian Sedimentary Basin” by Ghofrani and Atkinson (2020): Bulletin of the Seismological Society of America 111, 3459-3474.

Viegas, G., A. Baig, W. Coulter, T. Urbancic, 2012. Effective monitoring of reservoir-induced seismicity utilizing integrated surface and downhole seismic networks: First Break 30, 77-81.

Vilarrasa, V., S. De Simone, J. Carrera, A. Villaseñor, 2021. Unraveling the causes of the seismicity induced by underground gas storage at Castor, Spain: Geophysical Research Letters 48, e2020GL092038.

Wang, K., W. Ellsworth, G.C. Beroza, 2020. Revisting the Timpson induced earthquake sequence: a system of two parallel faults: Geophysical Research Letters 47, e2020GL089192.

Yeck, W.L., L.V. Block, C.K. Wood, V.M. King, 2015. Maximum magnitude estimations of induced earthquakes at Paradox Valley, Colorado, from cumulative injection volume and geometry of seismicity clusters: Geophysical Journal International 200, 322-336.

Yoon, C.E., Y. Huang, W.L. Ellsworth, G.C. Beroza, 2017. Seismicity during the initial stages of the Guy-Greenbrier, Arkansas, earthquake sequence: Journal of Geophysical Research 122, 9253-9274.

Zhou, P., H. Yang, B. Wang, J. Zhuang, 2019. Seismological investigations of induced earthquakes near the Hutubi underground gas storage facility: Journal of Geophysical Research 124, 8753-8770.